Journal of Catalysis **183,** 240–250 (1999)
Article ID jcat.1999.2418, available online at http://www.idealibrary.com on IDEAL®

Synthesis and Characterization of ZrO_2 as Acid–Basic Catalysts: Reactivity of 2-Methyl-3-butyn-2-ol

M. Angeles Aramendía, Victoriano Boráu, César Jiménez, José M. Marinas, Alberto Marinas, Andrés Porras, and Francisco J. Urbano

Department of Organic Chemistry, Faculty of Sciences, University of Cordoba, Avda San Alberto Magno s/n, E-14004 Cordoba, Spain

Received July 22, 1998; revised January 5, 1999; accepted January 8, 1999

Two ZrO_2-based catalysts have been synthesized by thermal treatment of a gel prepared from $ZrOCl_2 \cdot 8H_2O$. The effect of different preparation parameters on the final properties of the solids was studied. Textural characterization was carried out from nitrogen adsorption/desorption isotherms. XRD and FT-Raman spectroscopy have been used to elucidate the physical state of the catalysts. Their acid–base properties were studied following temperature programmed desorption–mass spectrometry and diffuse reflectance infrared Fourier transform techniques, by using pyridine, 2,6-dimethylpyridine and carbon dioxide as probe molecules. Both solids were tested for the 2-methyl-3-butyn-2-ol reaction by using two different procedures: (a) in a microcatalytic pulse reactor and (b) through isotherm and temperature programmed surface reactions in a flow reactor. In addition, temperature programmed oxidation and temperature programmed desorption experiments revealed that catalyst deactivation was caused by carbon deposition on the catalytic surface. Amphoteric selectivity for both solids, leading to 3-hydroxy-3-methyl-2-butanone and 3-methyl-3-buten-2-one, depends on the reaction temperature; thus, it is 92% at 225°C for a catalyst calcined at 400°C (ZrO_2–400VAC).

INTRODUCTION

The acid–base property is one of the most important surface chemical properties of metal oxide catalysts (1). In this sense, ZrO_2 is a promising material as catalyst, due to its amphoteric character as well as its thermal stability (2). At present, it has been applied as a catalyst to many organic reactions such as esterifications and olefin hydrogenations (3).

Textural and acid–base properties of ZrO_2 depend greatly on both the synthetic procedure and the calcination temperature (4). Modification of these properties by addition of alkaline metals (5) or sulfate ions (6, 7) as well as by mixing with other metal oxides (8) has also been studied extensively.

The normal procedure used to prepare ZrO_2 consists of calcination of its hydroxide (hydroxylated gel), which is prepared by hydrolysis of zirconium salts.

Zirconia is known to exist in monoclinic, tetragonal, and cubic phases and as an amorphous solid.The crystal forms of ZrO_2 depend on how the hydroxide is prepared and treated. Steaming of the hydroxide results in the formation of the monoclinic form, while a vacuum treatment leads to the tetragonal form (9). The tetragonal form presents better textural and acid–base properties than the monoclinic and, therefore, is the one most used in catalysis (10).

The studies on catalysis by solid acids are extremely numerous (11, 12). Several reviews have recently been published dealing with the use of solid acids as heterogeneous catalysts for the preparations of fine chemicals (13–16). An important characteristic of solid acids compared to liquid acids is that solid acids encompass different populations of sites differing in their nature and strength (17–21). Excellent reviews on catalysis by solid bases have been published (18–20). Finally, the cooperative behavior of surface sites with acid–base properties is an essential requirement for a wide range of catalytic reactions (21).

Due to the great number of reactions catalyzed by acid, basic, or acid–basic sites, the determination of number, strength, Brønsted or Lewis nature of the different acid–basic sites of solid catalysts, and softness and hardness of Lewis sites in these solid catalysts is very important. In a previous work, the acid characteristics of several catalysts were determined using a spectrophotometric procedure (22) with *n*-buthylamine in cyclohexane as probe molecule. Besides, temperature programmed desorption–mass spectrometry (TPD–MS) and TPD–diffuse reflectance infrared Fourier transform (DRIFT) techniques were designed to carry out the characterization of acid–basic sites. Test reactions are used as well to characterize acid–basic sites (23–25). Thus, Lauron-Pernot *et al.* (26–28) and other authors (29, 30) suggested the 2-methyl-3-butyn-2-ol (MBOH) reaction in order to characterize acid–base properties of solids.

In this work the textural and acid–base properties of two different zirconia catalysts are studied. The effect of the calcination temperature is discussed. Acid–base properties were studied by TPD–MS of preadsorbed probe

0021-9517/99 $30.00

molecules such as pyridine (total acidity), 2,6-dimethylpyridine (Brønsted acidity) and carbon dioxide (basicity). The reactivity of MBOH was used as a test reaction to compare the activity of the catalysts by two different procedures: (a) in a microcatalytic pulse reactor and (b) temperature programmed surface reactions (TPSR) in a flow reactor. In addition, isotherm reactions were carried out in order to obtain information about the solids. Finally, the catalyst deactivation was studied by techniques such as temperature programmed oxidation (TPO) and temperature programmed desorption (TPD) of strongly adsorbed species.

EXPERIMENTAL

Catalyst Synthesis

Zirconium hydroxide was prepared from 30 g of $ZrOCl_2 \cdot 8H_2O$ (Merck Art. 8917) and 1.5 L of distilled water. Next, NaOH 1 M was added until pH 6.8 was achieved. The gel was aged for 72 h and then filtered and air-dried for 24 h and placed in an oven at 110°C overnight.

ZrO_2 was obtained by calcination of the dried gel by heating *in vacuo* from room temperature to the final temperature (400 or 600°C) at a rate of 2°C/min. Then the final temperature was kept for 5 h and finally the solids were allowed to cool back to ambient temperature in a vacuum. The solids were named ZrO_2–400VAC and ZrO_2–600VAC, indicating their respective calcination temperatures.

Chemicals

2-Methyl-3-butyn-2-ol, pyridine and 2,6-dimethylpyridine were obtained from Aldrich.

Physical Characterization

The textural properties of solids (specific surface area, pore volume, and mean pore radius) were determined from nitrogen adsorption–desorption isotherms at liquid nitrogen temperature by using a Micromeritics ASAP-2000 instrument. Surface areas were calculated by the BET method (31), while pore distributions were determined by the BJH method (32). Prior to measurements, all samples were degassed at 350°C to 0.1 Pa.

X-ray investigation of the solids was carried out using a Siemens D-500 diffractometer provided with an automatic control and data acquisition system (DACO-MP). The patterns were run with nickel-filtered copper radiation ($\lambda = 1.5405$ Å) at 35 kV and 20 mA; the diffraction angle 2θ was scanned at a rate of 2°C/min.

FT-Raman spectra were obtained on a Perkin-Elmer 2000 NIR FT-Raman system with a diode pumped NdYAG laser (9394.69 cm^{-1}). It was operated at a resolution of 4 cm^{-1} over the range 3600–200 cm^{-1} to gather 64 scans.

DRIFT Experiments of Preadsorbed Probe Molecules

Diffuse reflectance infrared (DRIFT) experiments were conducted on a Bomen MB-100 instrument with an "environmental chamber" (Spectra-Tech). It was operated at a resolution of 8 cm^{-1} over the range 4000–400 cm^{-1} to gather 256 scans. In those experiments with preadsorbed molecules, each catalyst was cleaned by passing an Ar stream of 50 mL/min at 100°C for 30 min. The solids were saturated with the probe molecule and subsequently flushed with a stream of pure Ar (50 mL/min) at the saturation temperature for 2 h in order to avoid physisorption. The solid was then transferred to the DRIFT environmental chamber and spectra were obtained at three or four different temperatures (50, 100, 200, and 300°C). A temperature leveling time of 20 min was used.

Temperature-Programmed Desorption-Mass Spectrometry Experiments

TPD-MS experiments were carried out in an on-line device (see Fig. 1) with a VG Sensorlab quadrupole mass spectrometer. The optimum TPD conditions were as follows: heating rate, 10°C/min; Ar flow rate, 50 mL/min. The mass spectrometer, which was operated in the multiple ion monitoring (MIM) mode, was programmed to perform six scans per minute.

A quartz reactor (10 mm i.d., 200 mm long) was located in the middle of a furnace. The temperature of the furnace was controlled within an error of ±1°C. The output of the reactor was fitted on line to a VG Sensorlab mass spectrometer (Fisons Instrument, plc/VG quadrupoles) working in MIM mode. Monitored peaks and relative abundance were selected from *Eight Peak Index of Mass Spectra* (33).

The amines used as probe molecules to determine the acid properties of the solids were pyridine ($pK = 5.25$) and 2,6-dimethylpyridine ($pK = 7.3$). It is known that 2,6-dimethylpyridine is selectively adsorbed on Brønsted acid sites, but not on Lewis ones, because of the steric hindrance of two methyl groups, whereas sterically nonhindered pyridine is adsorbed on both Brønsted and Lewis (34, 35). The peaks used to quantify pyridine were the base peak ($m/z = 79$) and the secondary peak at $m/z = 52$ (80% relative abundance). The MS peaks chosen for 2,6-dimethylpyridine were the base peak ($m/z = 107$) and the secondary peak at $m/z = 66$ (60% abundance).

Carbon dioxide was the probe molecule used to determine the basic properties of the catalyst. The gases used for the CO_2 TPD–MS experiments were CO_2 and 5% CO_2 in argon, both of which were supplied by Sociedad Española de Oxígeno S.A. (>99.999%). Carbon dioxide was quantified by the base ($m/z = 44$) and secondary peaks ($m/z = 12$, 10% abundance). Calibration was performed by injecting pulses of pure CO_2 or 5% CO_2 in argon.

Prior to the adsorption of any probe molecule, each catalyst was cleaned by passing an Ar stream at 110°C at 50 mL/min for 30 min. The solids were then saturated by passing an amine/N_2 or CO_2/Ar stream (50 mL/min) at 25 and 50°C, respectively. Subsequently, a pure N_2 or Ar stream (50 mL/min) was passed at the saturation temperature for 2 h in order to remove any physisorbed molecules. Once a stable baseline was obtained, chemisorbed amine or CO_2 was desorbed by heating from saturation temperature to 600°C in a programmed fashion. The selected mass peaks were monitored throughout the process. Each experiment used ca. 100 mg of fresh catalyst. Full details of the TPD–MS method and equipment have been given elsewhere (36, 37).

NMR Spectroscopy

^{1}H MAS NMR spectra were obtained at 400.13 MHz on a Brucker ACP-400 spectrometer under an external magnetic field for 9.4 T. All measurements were made at room temperature although the samples had different thermal pretreatments which mentioned heating in a furnace for 24 h at 120°C and evacuation of the sample at 0.4 Pa at temperatures between 300 and 600°C. The samples contained in zirconia rotors were spun at the magic angle (54° 44′ relative to the external magnetic field) at 5 kHz. ^{1}H spectra were recorded after applying an excitation pulse of Π/2 (5 μs) with a 2-s interval between successive accumulations to avoid saturation effects (38). Tetramethylsilane (TMS) was used as external standard for the proton. The number of accumulations for the proton were 200.

Reactivity Tests

a. Reactions in microcatalytic pulse reactor. The catalytic processes were carried out in a microcatalytic pulse reactor (0.4 cm i.d. quartz tubular reactor) placed in the injection port of a gas chromatograph (Hewlett Packard Model 5890) equipped with a Supelcowax capillary column (30 m length and 0.20 mm i.d.) and with a flame ionization detector (FID). The catalyst was placed between two layers of glass wool. Previous to each run, it was pretreated *in situ* in the reactor at 200°C for 2 h under nitrogen (75 mL/min). The reactor temperature was then decreased to the reaction temperature. Data were collected over a wide range of experimental conditions: MBOH pulses, 0.5–2 μL; temperature, 160–350°C; N_2 flow, 80–110 mL/min. This procedure was repeated several times in order to follow the deactivation occurring during the first pulses.

In separate experiments, the reactions were carried out by using a GC-MS (HP5970 quadrupole mass spectrometer) in order to characterize the reaction products.

b. Temperature-programmed reaction experiments. TPSR, TPD, and TPO were performed in the device shown in Fig. 1.

TPSR were carried out in two temperature stages: an isotherm period (200°C for 30 min) and a second stage in which the temperature was raised from 200 to 600°C at a constant rate (10°C/min). The feed consisted of a nitrogen flow (50 mL/min) passed through a saturator with MBOH at 20°C. The whole process was monitored through the mass spectrometer.

For the TPD experiments, as soon as the TPSR reaction finished, the nitrogen flow was set to 50 mL/min N_2 and the catalyst was immediately cooled down to room temperature. Then the catalyst was kept at room temperature and nitrogen flow for at least 4 h to clean the surface from physisorbed species. Finally, the temperature was raised at a constant rate (10°C/min) from room temperature up to 600°C. The whole process was monitored through the mass spectrometer.

TPO were carried out in a way similar to that of TPD experiments, but using a 2% O_2/Ar flow (50 mL/min) during the temperature ramp.

RESULTS AND DISCUSSION

Physical Characterization of the Catalysts

The thermal analysis of the $Zr(OH)_2$ gel showed a continuous loss of water from 100°C. Between 300 and 450°C, a second step takes place. This second event has been attributed to the conversion of an amorphous material to a crystalline phase (9). The overall mass loss was about 15% of the initial gel.

Figure 2 shows the X-ray diffraction patterns of the dried gel (trace "*a*") as well as those of both ZrO_2 samples studied in this work (traces "*b*" and "*c*" for the solids ZrO_2–400VAC and ZrO_2–600VAC, respectively). Diffractogram "*a*" is typical of an amorphous solid, showing broad bands. On the contrary, pattern "*c*" presented numerous sharp bands indicating that ZrO_2–600VAC is a crystalline solid. This pattern corresponding to ZrO_2–600VAC was found to be composed of bands corresponding to two different crystalline phases: a minor tetragonal phase and a main monoclinic phase (baddeleyite). The tetragonal phase is metastable and reverts to the monoclinic, which is, therefore, the dominant phase. Catalyst ZrO_2–400VAC is not very crystalline, showing weak bands corresponding to the tetragonal phase.

FT-Raman spectra confirm the results obtained from XRD. Raman spectroscopic information is particulary valuable for distinguishing the different phases of zirconia. In fact, tetragonal and cubic phase unambiguous assignment is not possible from XRD alone (39, 40). Kilo *et al.* (39) reported the Raman frequencies observed for the modifications of zirconia. The most striking difference between the Raman spectra of stable monoclinic and metastable tetragonal zirconia is the presence of a band at ca. 380 cm^{-1} in the spectrum of the former modification and a characteristic band at 255–265 cm^{-1} in the spectrum of the latter

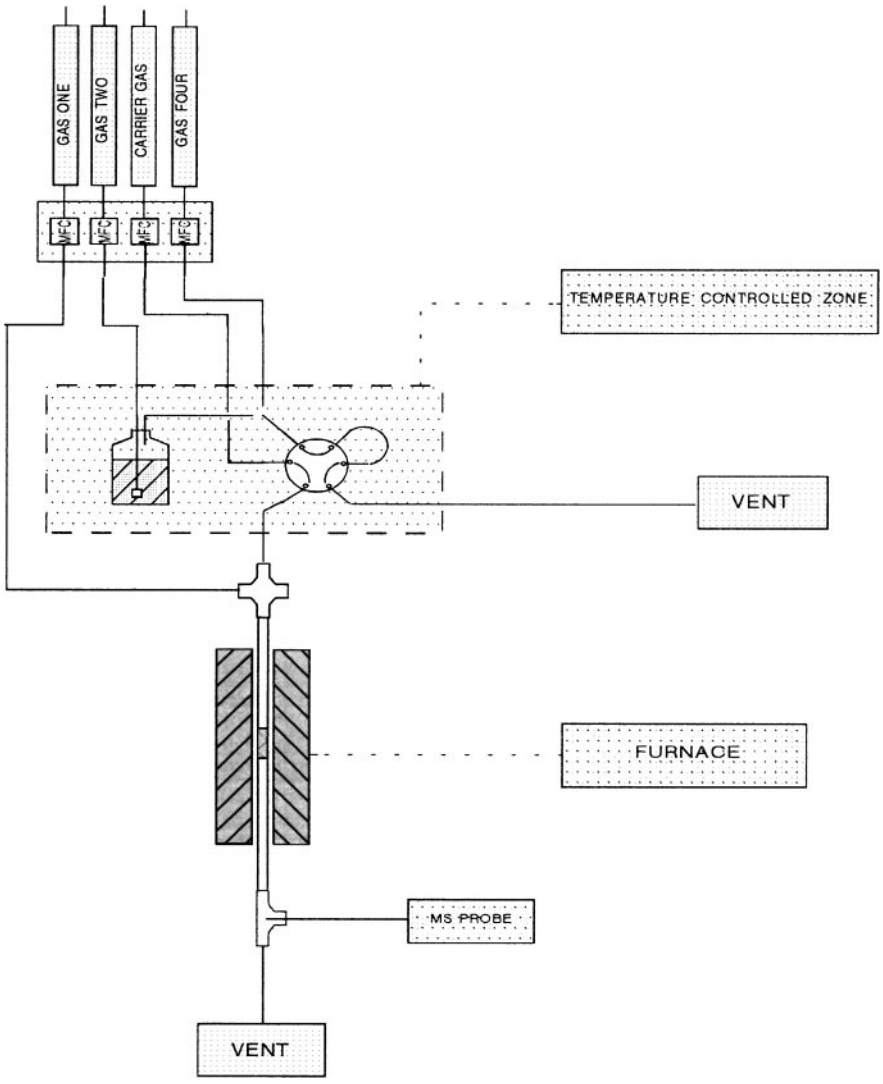

FIG. 1. Experimental device.

modification. Figure 3 presents the Raman spectra corresponding to the dried gel (trace "*a*"), as well as the catalysts ZrO_2–400VAC and ZrO_2–600VAC (traces "*b*" and "*c*," respectively). According to the XRD results, the Raman spectrum of the dried gel correspond to an amorphous solid. On the other hand, the spectrum of the ZrO_2–600VAC shows characteristic peaks of the monoclinic phase, while those typical of the tetragonal phase (e.g., that at 255–265 cm^{-1}) appear only as small shoulders. The ZrO_2–400VAC shows poor crystallinity, which can be assigned to the tetragonal phase.

Nitrogen adsorption–desorption isotherms obtained for both zirconium oxides (ZrO_2–400VAC and ZrO_2–600VAC) are shown in Fig. 4. Both catalysts present isotherms with closed and well defined hysteresis loops. The isotherms are Type IV in the Brunauer, Deming, Deming, and Teller (BDDT) classification associated with mesoporous solids (41, 42). However, the shape of the hysteresis loops in the isotherms of Figs. 4A and 4B changes from intermediate between A and E to A type according to the classification of De Boer (43) (H1 and H2 following the IUPAC nomenclature). In a previous work (44), it was found that a zirconium oxide calcined at 300°C (called ZrO_2–300VAC) showed E type hysteresis, which is often associated with "ink-bottle" pores, spheroidal cavities, or voids among close-packed spherical particles. On the other hand, A-type hysteresis (ZrO_2–600VAC) is characteristic of cylindrical pores. It seems, therefore, that the zirconia samples prepared are essentially mesoporous and contain spherically shaped pores which are gradually smoothed into cylindrically shaped pores on calcination (4).

Surface area, pore volume and mean pore radius are compiled in Table 1. The effect of the calcination temperature on surface area is dramatic as reported in the

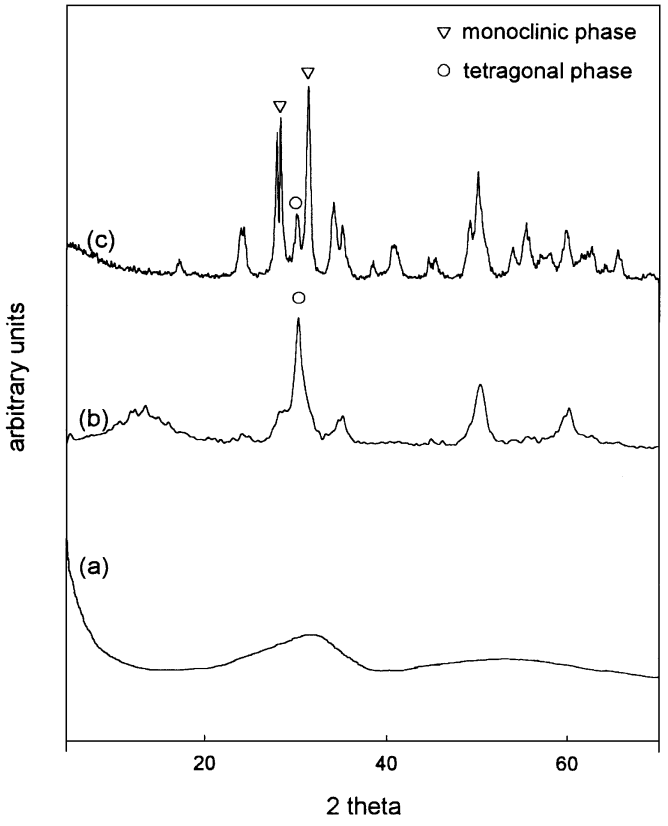

FIG. 2. X-ray diffraction patterns corresponding to ZrOH gel (a) and the catalysts ZrO_2–400VAC (b) and ZrO_2–600VAC (c).

bibliography (2). The BET surface area decreases from 110 to 28 m^2/g when the calcination temperature goes from 400 to 600°C. Mercera *et al.* (4) identified two possible processes as being responsible for the changes occurring in the pore structure and surface area on increasing calcination temperature: crystallite growth and the accompanying phase transformation on the one hand and sintering between the crystallites (neck formation and growth) on the other.

The temperature causes severe loss of surface area, as seen in Table 1, as well as transformation in the structure of the solid, as proved by XRD and FT-Raman experiments. The catalyst ZrO_2–400VAC is an almost amorphous, high surface area solid, whereas ZrO_2–600VAC exhibits a low surface area and a monoclinic structure.

TABLE 1

Textural Properties of the Catalysts

Catalyst	Precursor	S_{BET} ($m^2\ g^{-1}$)	V_p ($mL\ g^{-1}$)	r_p (Å)
ZrO_2–400VAC	$ZrOCl_2 \cdot 8H_2O$	110	0.15	19
ZrO_2–600VAC	$ZrOCl_2 \cdot 8H_2O$	28	0.11	155

Note. Specific surface area (S_{BET}), pore volume (V_p), and pore mean radius (r_p) obtained for the solids used in this work.

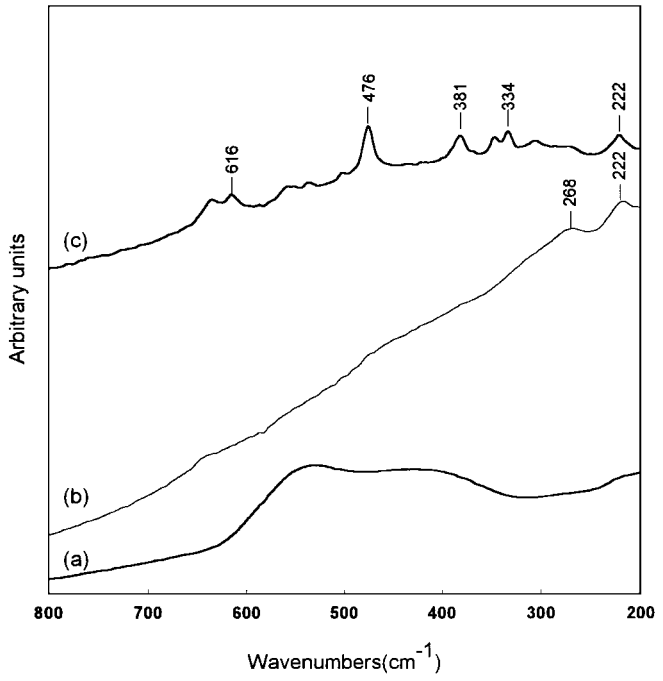

FIG. 3. FT-Raman spectra corresponding to zirconium dried gel (trace *a*), as well as the catalysts ZrO_2–400VAC and ZrO_2–600VAC (traces *b* and *c*, respectively).

Acid–Basic Properties

Pyridine (PY), 2,6-dimethylpyridine (DMPY), and carbon dioxide were used as probe molecules to determine overall acidity, Brønsted acidity, and overall basicity of the catalysts from TPD–MS of preadsorbed probe molecules. Table 2 presents the results obtained for the solids used in this study. The solid calcined at 400°C presents higher acidity and basicity than that calcined at 600°C. However, catalyst ZrO_2–600VAC exhibits a smaller but stronger basic-site population than ZrO_2–400VAC. In conclusion, it is clear that calcination temperature is a crucial factor in obtaining ZrO_2-based solids with good acid–base properties.

This TPD–MS method allows us to determine, in addition to the number of basic and acid sites, the relative strength of those sites. Figures 5, 6, and 7 show the TPD–MS profiles obtained for pyridine, 2,6-dimethylpyridine, and CO_2

TABLE 2

Acid–Basic Properties Determined by Temperature-Programmed Desorption-Mass Spectrometry (TPD–MS) for the Solids Used in This Work

Catalyst	Acidity ($\mu mol\ g^{-1}$)			Basicity ($\mu mol\ g^{-1}$), CO_2
	Brønsted DMPY	Lewis PY–DMPY	Total PY	
ZrO_2–400VAC	43	16	59	104
ZrO_2–600VAC	25	5	30	22

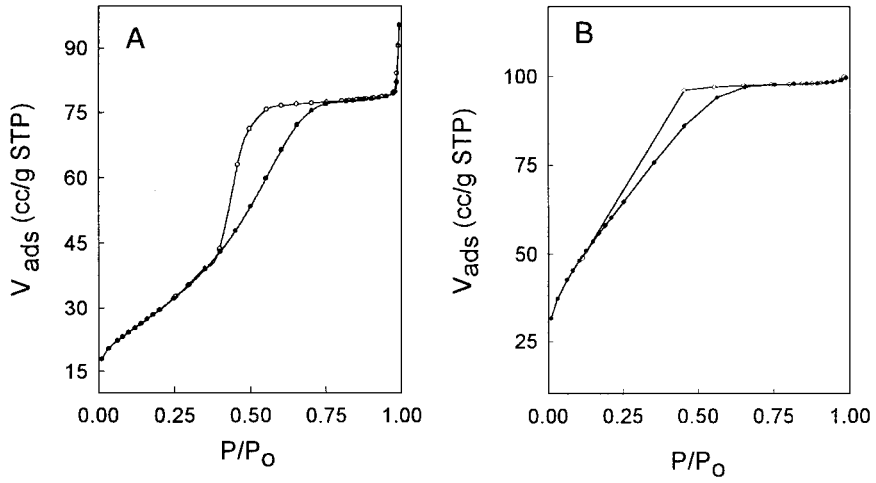

FIG. 4. Nitrogen adsorption–desorption isotherms obtained at liquid nitrogen temperature for the catalysts ZrO_2–400VAC (A) and ZrO_2–600VAC (B) (●, adsorption band; ○, desorption band).

preadsorbed on both ZrO_2 based catalysts. As far as overall acidity (Fig. 5) is concerned, catalyst ZrO_2–400VAC shows a single peak of desorption of pyridine at 135°C, whereas ZrO_2–600VAC exhibits not only this peak but also another one at 161°C. The peak at 135°C coincides with the peak shown in the DMPY TPD–MS profile (Fig. 6) and therefore is assigned to Brønsted sites. The peak at 161°C does not appear in the profile corresponding to DMPY TPD–MS (Fig. 6); thus, it is assigned to Lewis acid sites. From Figs. 5 and 6 we can conclude that the acidity of ZrO_2–400VAC is higher than that of ZrO_2–600VAC, being Brønsted sites higher than Lewis ones for both solids. The range of acid strength is broader for ZrO_2–400VAC than for ZrO_2–600VAC. The change on calcining in the number of acid sites but not in their types can be mainly assigned to the dramatic reduction in surface area rather than to morphological changes in the structure.

The effect of calcination on the basicity is much more intense than on surface acidity. CO_2 TPD–MS profiles (Fig. 7) indicate that the solid calcined at 400°C (ZrO_2–400VAC)

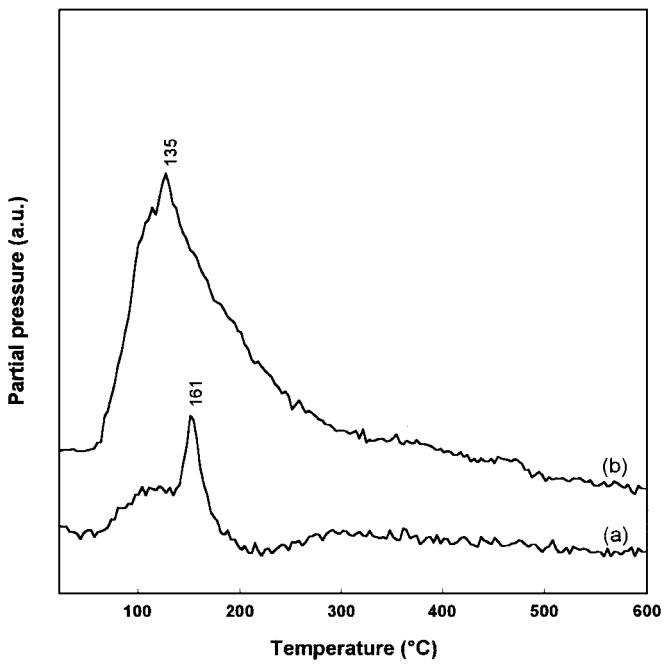

FIG. 5. Temperature programmed desorption–mass spectrometry profiles of preadsorbed pyridine over the catalysts ZrO_2–600VAC (a) and ZrO_2–400VAC (b).

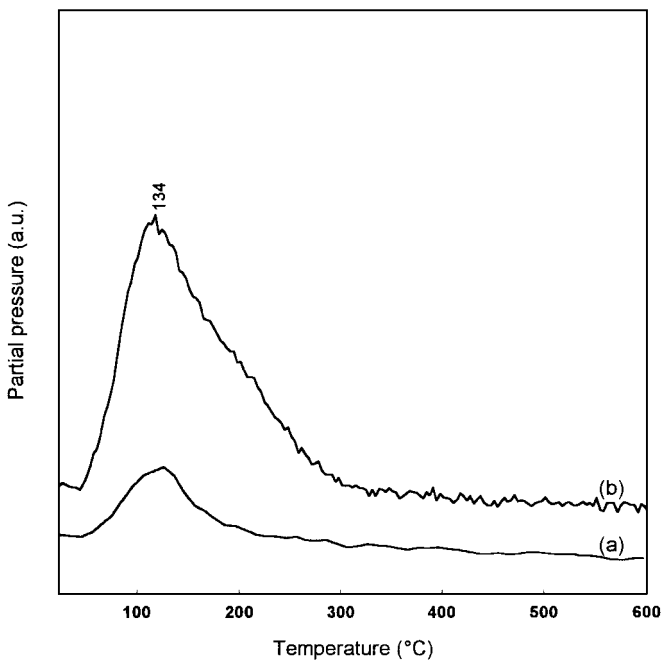

FIG. 6. Temperature programmed desorption–mass spectrometry profiles of preadsorbed 2,6-dimethylpyridine over the catalysts ZrO_2–600VAC (a) and ZrO_2–400VAC (b).

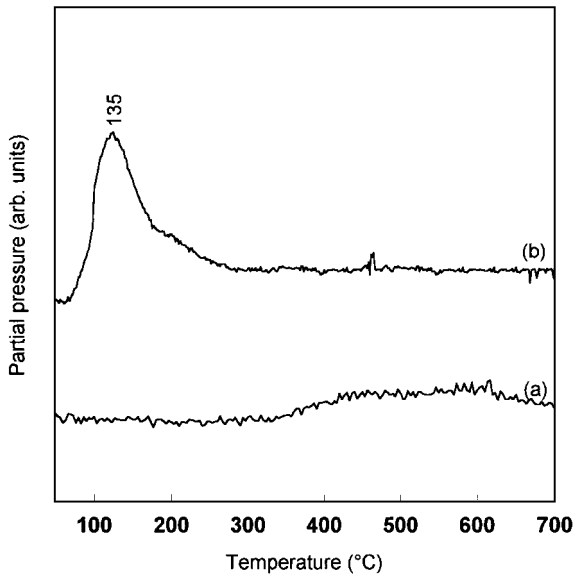

FIG. 7. Temperature programmed desorption–mass spectrometry profiles of preadsorbed CO_2 over the catalysts ZrO_2–600VAC (a) and ZrO_2–400VAC (b).

has not only a greater number of basic sites but also a different distribution of strength as compared to ZrO_2–600VAC. In this sense, ZrO_2–400VAC presents basic sites of low strength (desorbing CO_2 in the range 100–200°C). However, the solid calcined at 600°C (ZrO_2–600VAC) has lost those weak basic sites, showing only a slight increase of the baseline in the range 350–650°C related to a broad population of basic sites of great strength. The reason for this change in the acid–base properties—more marked on basic sites than on acid sites—may be related to a morphological change in the catalyst crystal phase (from amorphous and tetragonal to monoclinic) rather than to the mere reduction in surface area. The nature of the acid sites was the same in both solids; only their numbers differed. On the other hand, basic sites on the two solids differed not only in number and strength, but also in nature.

The study of surface acid and basic properties in both ZrO_2-based catalysts is completed with the DRIFT spectra of pyridine and carbon dioxide adsorbed on the catalysts at room temperature.

Marinas *et al.* (34) found that pyridine is adsorbed on Brønsted and Lewis acid sites showing bands at around 1450, 1490, and 1590 cm^{-1}. The first and third ones correspond to the adsorption on Brønsted sites while the second is assigned to adsorption on Lewis acid sites. Both solids exhibit all three bands in agreement with data from PY and DMPY TPD–MS experiments that indicate that catalysts present both Brønsted and Lewis acid sites. Spectra obtained at temperature over ambient also confirm that the acid strengths of the two catalysts are similar since infrared bands disappear at about the same temperature for both.

On the other hand, the DRIFT spectra of preadsorbed CO_2 allow research on the different types of surface species formed upon CO_2 adsorption on ZrO_2-based catalysts (45–47). DRIFT spectra corresponding to the solid ZrO_2–600VAC are of poor quality due to the small number of basic sites on this catalyst. The main species observed on the surface are unidentate carbonate (bands at 1304 and 1404 cm^{-1}) and bidentate carbonate (at 1632 cm^{-1}), the last being the most abundant surface species. A detailed study of surface species after carbon dioxide adsorption on different oxide type catalysts has been published in a previous work (37).

^1H MASNMR

Figure 8 shows the ^1H MASNMR spectra for catalysts ZrO_2–400VAC and ZrO_2–600VAC after treatment for 24 h in a furnace at 120°C (a and b) and at room temperature (c and d). It was found that ZrO_2–400VAC is the catalyst that shows the greater number of OH groups. However, a wider range of distribution is observed in ZrO_2–600VAC. The small number of sites at $\delta = 0.85$ and $\delta = 1.71$ displayed by ZrO_2–600VAC could correspond to the few but strong basic sites detected for this catalyst by CO_2–TPD–MS.

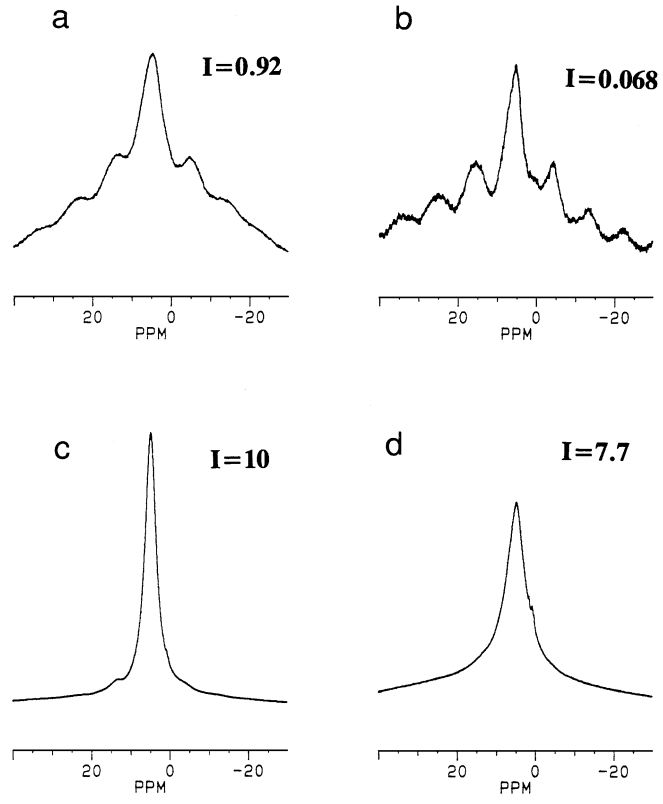

FIG. 8. ^1H NMRMAS spectra of zirconia based catalysts: (a) ZrO_2–400VAC heated at 120°C in a furnace. (b) ZrO_2–600VAC heated at 120°C in a furnace. (c) ZrO_2–400VAC at room temperature. (d) ZrO_2–600VAC at room temperature.

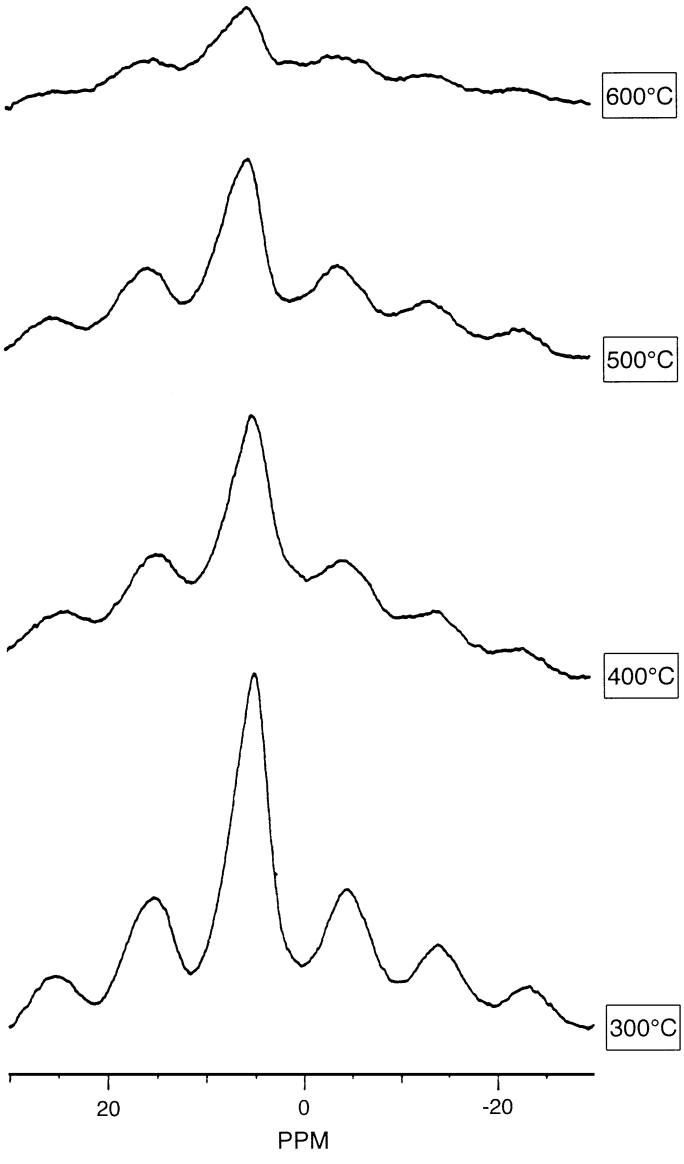

FIG. 9. ^{1}H NMRMAS spectra of zirconia heated *in vacuo* for 5 h at 300, 400, 500, and 600°C. The scale is the same for all the spectra.

^{1}H MASNMR spectra for zirconia heated *in vacuo* at temperatures between 300 and 600°C are shown in Fig. 9. It is important to emphasize that even though the number of OH groups decreases as the temperature increases, these groups are detected at temperatures as high as 600°C.

Reactivity of 2-Methyl-3-butyn-2-ol

The MBOH reaction has been proposed by several authors as a test reaction in order to characterize a solid as acid, basic, or amphoteric. When MBOH makes contact with a solid, it can undergo three different reactions, leading to the main products shown in Scheme 1.

Reactions in microcatalytic pulse reactor. The catalytic runs were carried out in absence of diffusional influences (boundary layer, internal and external mass transfer processes) through the choice of suitable operating variables, especially space velocity (changing the catalyst weight and the carrier gas) and particle size. Furthermore, the catalytic runs have been carried out at different weight ratios of catalyst to the substrate introduced (pulses in the range 0.2–1.5 μL), showing that conversion was almost unchanged, which determines the first-order reaction process.

Hence, in absence of diffusional influences and in the range 160–230°C, the requirements of Bassett–Habgood kinetic treatment (48) for first-order kinetic processes are satisfied. Thus, the rate determining step is the surface reaction,

$$\ln[1/1 - X_p] = RTK(W/F),$$

where X_p is MBOH conversion, K the pseudokinetic constant, W the catalyst weight, and F the flow-rate of the carrier gas. On the contrary, as the temperature rises, very high conversions and several secondary products, such as trimethylbencenes or 3,5,5-trimethyl-2-cyclohexen-1-one, are found and the Bassett and Habgood equation is not fulfilled. In the range 160–200°C, in which the Bassett and Habgood equation is followed, the change in amphoteric selectivity ($S_{amp} = S_{HMB} + S_{MIPK}$) and relative selectivity ($S_{rel} = S_{MIPK}/S_{HMB}$) with the temperature and the carrier gas flow (from 80 to 120 ml/min) was studied. In all cases, S_{rel} increases drastically with the temperature, mainly due to the increase in 3-methyl-3-buten-2-one (MIPK), as changes in 3-hydroxy-3-methyl-2-butanone (HMB) are not significant. At the same temperature, that selectivity increases as the carrier gas flow decreases. It is important to point out that the first pulse gives very high conversion with MBYNE as the main product and a low ratio of MIPK. During the other four pulses, MBYNE disappears and growing quantities of HMB are formed as MIPK hardly changes.

Results found for a range of temperatures between 225 and 300°C and a total flow of 75 mL/min are shown in Table 3. Total conversion and selectivity in MBYNE+prenal (acid sites), acetone+acetylene (basic sites), as well as MIPK and HMB (acid–base pair sites) as a function of

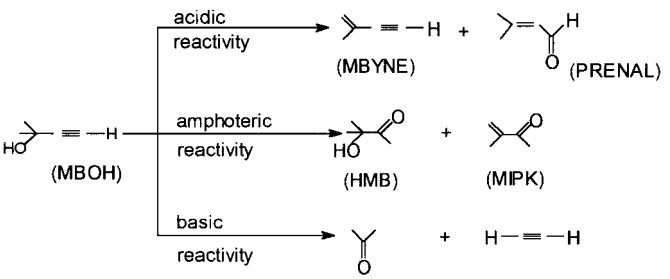

SCHEME 1. Overall reaction scheme (26). MBOH, 2-methyl-3-butyn-2-ol; MBYNE, 3-methyl-3-buten-1-yne; PRENAL, 3-methyl-2-buten-1-al; HMB, 3-hydroxy-3-methyl-2-butanone; MIPK, 3-methyl-3-buten-2-one.

TABLE 3

Comparison between Selectivity to Both ZrO_2 Based Catalysts, at Three Different Temperatures

Catalyst	Temperature (°C)												Acid sites/Basic sites
	225				250				300				
	S_{MIPK}	S_{HMB}	S_{amp}	S_{rel}	S_{MIPK}	S_{HMB}	S_{amp}	S_{rel}	S_{MIPK}	S_{HMB}	S_{amp}	S_{rel}	
ZrO_2–400VAC	0	91.75	91.75	0	23.62	50.29	73.91	31.96	26.01	12.35	38.36	67.81	0.50
ZrO_2–600VAC	0	87.91	87.91	0	17.21	60.45	77.66	22.16	28.93	33.33	62.26	46.47	1.36

Note. S_{MIPK}, selectivity to MIPK; S_{HMB}, selectivity to HMB; S_{amp}, amphoteric selectivity ($S_{amp} = S_{MIPK} + S_{HMB}$); S_{rel}, relative selectivity ($S_{rel} = S_{MIPK}/S_{amp}$). Acid sites/Basic sites: ratio between both populations.

temperature for catalyst ZrO_2–400VAC is represented in Fig. 10.

From the study of Table 3, it can be concluded that within this range of temperatures, ZrO_2–400VAC is the catalyst with higher amphoteric selectivity at a lower temperature and, at the same time, the one for which the selectivity decreases with the temperature at a faster rate. S_{rel} and total conversion increases with the temperature. On the other hand, some experiments were carried out adding 2% water to MBOH, finding that the relative selectivity in HMB doubles the selectivity in MIPK. This increase is not produced at the expense of MIPK, which only needs the addition of a water molecule to produce one of HMB, but instead at the expense of MBYNE which can lead to HMB by the addition of two molecules of water (see Scheme 2).

Temperature-programmed experiments. To initially check the activity of our catalysts for MBOH decomposition several experiments at programmed and isothermal temperature (TPSR and ITSR) were carried out. The results confirmed those obtained from the pulse reaction. Moreover, TPD and TPO experiments performed after each reaction gave some important information about the causes of deactivation of the catalysts. MBOH conversion at 250°C on catalyst ZrO_2–600VAC is represented in Fig. 11. Like in pulse reactions, there is a fast and strong initial deactivation, after which the catalyst reaches stability.

TPD and TPO experiments carried out after isothermal reaction at low temperature have proved that deactivation is caused by strong retention of surface species (mainly MIPK). As the reaction temperature increases, the amount of MIPK retained by the catalyst decreases. At 600°C, no retained species are detected by TPD–MS experiments.

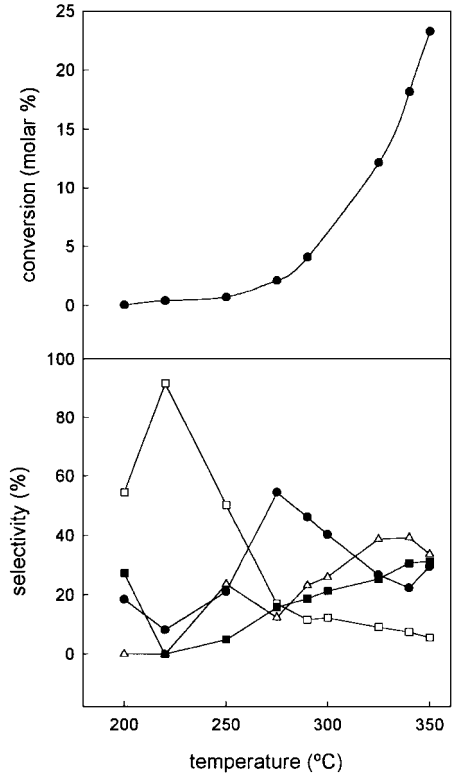

FIG. 10. Total conversion and selectivity in MBYNE+prenal (●), acetone+acetylene (■), MIPK (△), and HMB (□) as a function of temperature for catalyst ZrO_2–400VAC.

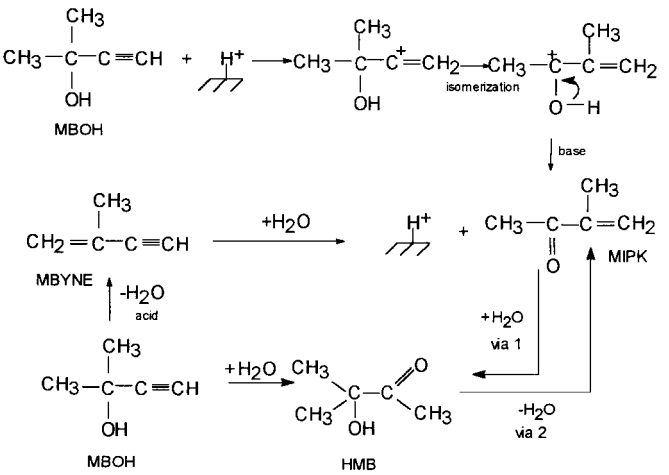

SCHEME 2. Reaction scheme for the two main products (MIPK and HMB) over acid–base pair sites.

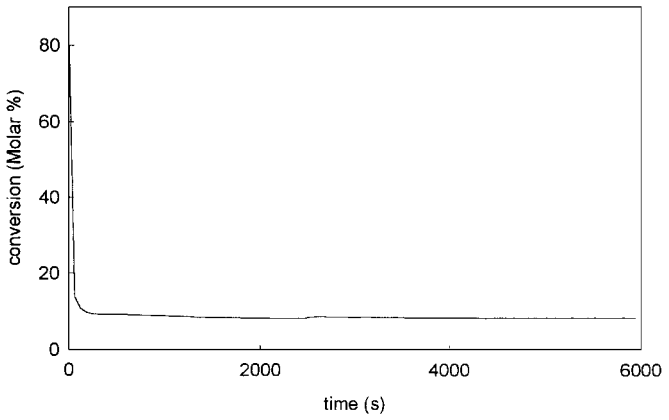

FIG. 11. Deactivation curve at 250°C on catalyst ZrO_2–600VAC in an IR-MS experiment.

TPO experiments carried out after temperature programmed reaction (final temperature 600°C) have proved that deactivation is caused by carbon deposition in both catalysts. The CO_2 area as well as the regeneration temperature were very similar in both catalysts (see Fig. 12).

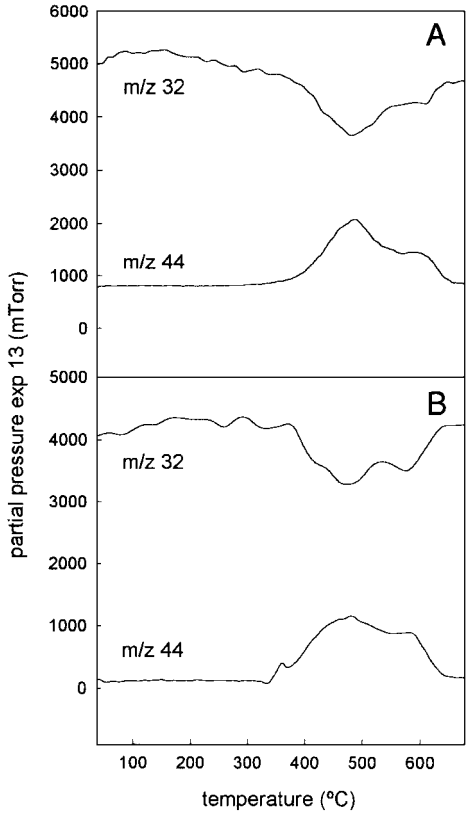

FIG. 12. Temperature programmed oxidation (TPO) profiles obtained for the catalyst ZrO_2–400VAC (A) and ZrO_2–600VAC (B), performed after keeping the catalyst under TPSR of MBOH. CO_2 ($m/z = 44$) and O_2 ($m/z = 32$) signals.

Regarding these experiments, and since deactivation increases with temperature, it seems that deactivation at high temperatures (about 400°C) is due to carbon deposition while at low temperatures (around 300°C), both carbon deposition and fundamentally strongly adsorbed reactants are what cause catalyst deactivation.

CONCLUSIONS

The results obtained in this work and the above interpretation allow us to draw the following conclusions:

(a) The calcination temperature is crucial to determine the structural, textural, and surface chemical properties of the ZrO_2 obtained. Calcination at 400°C led to an almost amorphous solid, whereas calcination at 600°C gave a mixture of tetragonal and monoclinic solid. A dramatic reduction in the surface area for the ZrO_2–600VAC solid was obtained. Calcination at 600°C led to a reduction in the number of acid sites without any change in the strength distribution. However, calcination at 600°C induced changes in the basic strength of the remaining sites: there were fewer but stronger sites than in the solid calcined at 400°C. The acidity lost could be due to surface area reduction by the sintering of the crystallites, while phase transformation (from amorphous to crystalline) is responsible for the change in the strength distribution of basic sites.

(b) The effect of temperature on selectivity for both catalysts must be taken into account in order to use the MBOH reaction as a catalytic test. Thus, the range from 160 to 210°C was the most appropriate.

(c) Relative selectivity increases drastically with the temperature, mainly due to the increase in MIPK since changes in HMB are not significant. At the same temperature, that selectivity increases as the carrier gas flow decreases.

(d) Isotherm reaction profiles showed an initial deactivation period that depended on the reaction temperature. TPD and TPO experiments performed after an isothermal run indicated that deactivation at high temperatures (about 400°C) was related to carbon deposition, while at low temperatures (around 200°C), both carbon deposition and strongly adsorbed species caused catalyst deactivation.

ACKNOWLEDGMENTS

The authors gratefully acknowledge the funding of this research by the Junta de Andalucía and the DGESIC in the framework of Project PB97-0446. The staff at the Mass Spectrometry and RMN Services of the University of Córdoba are also acknowledged for their kind technical assistance in the experiments.

REFERENCES

1. Tanabe, K., Misono, M., Ono, Y., and Hattori, H., "New Solid Acids and Bases." Kodansha, Tokyo; Elsevier, Amsterdam, 1989.
2. Yamaguchi, T., *Catal. Today* **20**, 199 (1994).

3. Tanabe, K., and Yamaguchi, T., *Catal. Today* **20**, 185 (1994).
4. Mercera, P. D. L., Van Ommen, J. G., Doesburg, E. B. M., Burggraaf, A. J., and Ross, J. R. H., *Appl. Catal.* **57**, 127 (1990).
5. Matsuda, T., Sasaki, Y., Miura, H., and Sugiyama, K., *Bull. Chem. Soc. Jpn.* **58**, 1041 (1985).
6. Norman, C. J., Goulding, P. A., and McAlpine, I., *Catal. Today* **20**, 313 (1994).
7. Rezgui, S., Jentoft, R. E., and Gates, B. C., *Catal. Lett.* **51**, 229 (1998).
8. Turlier, P., Dalmon, J. A., Martin, G. A., and Vergnon, P., *Appl. Catal.* **29**, 305 (1987).
9. Murase, Y., and Kato, E., *Yogyo Kyokaishi* **86**, 226 (1978).
10. Shibagaki, M., *Fine Chem.* **21**, 5 (1992).
11. Tanabe, K., "Solid Acids and Bases." Kodansha, Tokyo; Academic Press, New York, 1970.
12. Guisnet, M. R., *Acc. Chem. Res.* **23**, 392 (1990).
13. Corma, A., *Chem. Rev.* **95**, 559 (1995).
14. Venuto, P. B., *Microporous Mater.* **2**, 297 (1994).
15. Feast, S., and Lercher, J. A., *Stud. Surf. Sci. Catal.* **75**, 127 (1993).
16. Weitkamp, J., Weiss, U., and Ernst, S., *Stud. Surf. Sci. Catal.* **94**, 363 (1995).
17. Corma, A., and García, H., *Catal. Today* **38**, 257 (1997).
18. Hattori, H., *Chem. Rev.* **95**, 527 (1993).
19. Hattori, H., *Stud. Surf. Sci. Catal.* **78**, 35 (1993).
20. Ono, Y., and Baba, T., *Catal. Today* **38**, 321 (1997).
21. Iglesia, E., Barton, D. G., Biscardi, J. A., Gines, M. J. L., and Soled, S. L., *Catal. Today* **38**, 339 (1997); Tanabe, K., *Trends Anal. Chem.* **13**, 164 (1994).
22. Campelo, J. M., García, A., Gutiérrez, J. M., Luna, D., and Marinas, J. M., *Can. J. Chem.* **61**, 544 (1989).
23. Haffad, D., Kameswari, U., Bettahar, M. M., Chambellan, A., and Lavalley, J. C., *J. Catal.* **172**, 85 (1997).
24. Berkani, M., Lemberton, J. L., Marczewski, M., and Perot, J., *Catal. Lett.* **31**, 405 (1995).
25. Blaser, H. U., Casagrande, B., and Siebenhaar, B., *Stud. Surf. Sci. Catal.* **108**, 595 (1997).
26. Lauron-Pernot, H., Luck, F., and Popa, J. M., *Appl. Catal.* **78**, 213 (1991).
27. Audrey, F., Hogan, P. E., Saussey, J., Lavalley, J. C., Lauron-Pernot, H., and Legovic, A. M., *J. Catal.* **168**, 471 (1997).
28. Lahousse, C., Bachelier, J., Lavalley, J. C., Lauron-Pernot, H., and Legovic, A. M., *Pure Appl. Chem.* **66**, 1509 (1994).
29. Huang, M., and Kaliaguine, S., *Stud. Surf. Sci. Catal.* **78**, 559 (1993); Huang, M., and Kaliaguine, S., *Catal. Lett.* **18**, 373 (1993).
30. Lippert, S., Baumann, W., and Thomke, K., *J. Mol. Catal.* **69**, 199 (1991).
31. Brunauer, S., Emmett, P. H., and Teller, E., *J. Am. Chem. Soc.* **60**, 309 (1939).
32. Barret, E. P., Joyner, L. S., and Halenda, P. P., *J. Am. Chem. Soc.* **73**, 373 (1951).
33. "Eight Peak Index of Mass Spectra." The Royal Society of Chemistry, Nottingham, 1983.
34. Bautista, F. M., Campelo, J. M., García, A., Luna, D., Marinas, J. M., and Urbano, M. R., *J. Mater. Chem.* **4**, 311 (1994).
35. Ziolek, M., Kujawa, J., Saur, O., Aboulayt, A., and Lavalley, J. C., *J. Mol. Catal.* **A112**, 125 (1996).
36. Aramendía, M. A., Borau, V., Jiménez, C., Marinas, J. M., Porras, A., and Urbano, F. J., *Rapid Commun. Mass Spectrom.* **8**, 599 (1994).
37. Aramendía, M. A., Borau, V., Jiménez, C., Lafont, F., Marinas, J. M., Porras, A., and Urbano, F. J., *Rapid. Commun. Mass Spectrom.* **9**, 193 (1995).
38. Akkitt, J. W., *Annu. Rep. NMR Spectrosc.* **A5**, 465 (1972).
39. Kilo, M., Schild, C., Wokaun, A., and Baiker, A., *J. Chem. Soc. Faraday Trans.* **88**, 1453 (1992).
40. Yashima, M., Ohtake, K., Kakihana, M., Arashi, H., and Yoshimura, M., *J. Phys. Chem. Solids* **57**, 17 (1996).
41. Greg, S. J., and Sing, K. S. W., "Adsorption, Surface Area and Porosity," 2nd ed. Academic Press, London, 1982.
42. Sing, K. S. W., Everett, D. H., Haul, R. A. W., Moscou, L., Pierotti, R. A., Rouquerol, and Siemieniewska, T., *Pure Appl. Chem.* **57**, 603 (1995).
43. de Boer, J. J., Everett, D. H., and Stone, F. S. (Eds.), "The Structure and Properties of Porous Materials," p. 68. Butterworths, London, 1965.
44. Aramendía, M. A., Borau, V., Jiménez, Marinas, J. M., Porras, A., and Urbano, F. J., *J. Chem. Soc. Faraday Trans.* **93**, 1431 (1997).
45. Bianchi, D., Gass, J. L., Khalfallah, M., and Teichner, S. J., *Appl. Catal.* **101**, 297 (1993).
46. Bianchi, D., Chafik, T., Khalfallah, M., and Teichner, S. J., *Appl. Catal.* **105**, 223 (1993).
47. Bianchi, D., Chafik, T., Khalfallah, M., and Teichner, S. J., *Appl. Catal.* **112**, 219 (1994).
48. Bassett, D., and Habgood, H. W., *J. Phys. Chem.* **64**, 769 (1960).